Vibration Isolation of Precision Payloads: A Six-axis Electromagnetic Relaxation Isolator

B. de Marneffe, M. Avraam, A. Deraemaeker, M. Horodinca, A. Preumont*
Active Structures Laboratory, Université Libre de Bruxelles
CP. 165-42, 50 Av. F.D. Roosevelt, B-1050 Brussels, Belgium
e-mail: andre.preumont@ulb.ac.be

August 22, 2008

Abstract

This paper describes a passive 6-axis vibration isolation system for space applications. The system consists of a Stewart platform with cubic architecture; each leg is equipped with an electromagnetic transducer connected to a RL circuit. The system behaves like a relaxation isolator and its transmissibility exhibits an asymptotic decay rate of -40 dB/decade. The performances are very similar to that of an active isolator based on a sky-hook controller.

1 Introduction

Space telescopes and precision payloads are subject to jitter due to the unbalanced masses of the attitude control reaction wheels or gyros. The performance of the instruments may be improved by inserting one or several isolators in the transmission path between the disturbance source and the payload [1,2]. If the isolator is designed in such a way that its transmissibility exhibits a decay rate of -40 dB/decade, the jitter can be reduced by a factor 100 by selecting the isolator corner frequency, f_0, one decade lower than the first flexible mode of the payload, f_n (Fig.1). Extremely sensitive payloads may even involve several isolation layers. [1]

*Associate Fellow AIAA

[1]The future James Webb Space Telescope, JWST will involve two isolation layers, *(i)* the wheel isolator supporting six reaction wheels, with corner frequencies at 7 Hz for rocking and 12 Hz for translation and *(ii)* a 1 Hz passive isolator at the interface between the telescope deployment tower and the spacecraft bus [3].

1.1 Interaction isolator/attitude control

There are several possible locations for the isolator, depending on the spacecraft architecture (Fig.2). If the attitude control wheels are packed in a single assembly (RWA), the isolator may be placed between the RWA and the spacecraft bus (Fig.2.b). Another option consists in placing the isolator between the spacecraft bus and the instrument (Fig.2.c); in this alternative, the rotating wheels are rigidly attached to the spacecraft bus. The additional compliance introduced by the vibration isolator has a major impact on the low frequency dynamics of the system and its interaction with the attitude control system must be taken into account. The most favorable situation is that where the attitude control actuators and the attitude sensors (star trackers) are both rigidly attached to the spacecraft bus (collocated). For non-collocated situations, the stability of the control system requires that the corner frequency f_0 of the isolator be one decade above the attitude control bandwidth, f_c; altogether,

$$f_c \sim 0.1 f_0 \sim 0.01 f_n \tag{1}$$

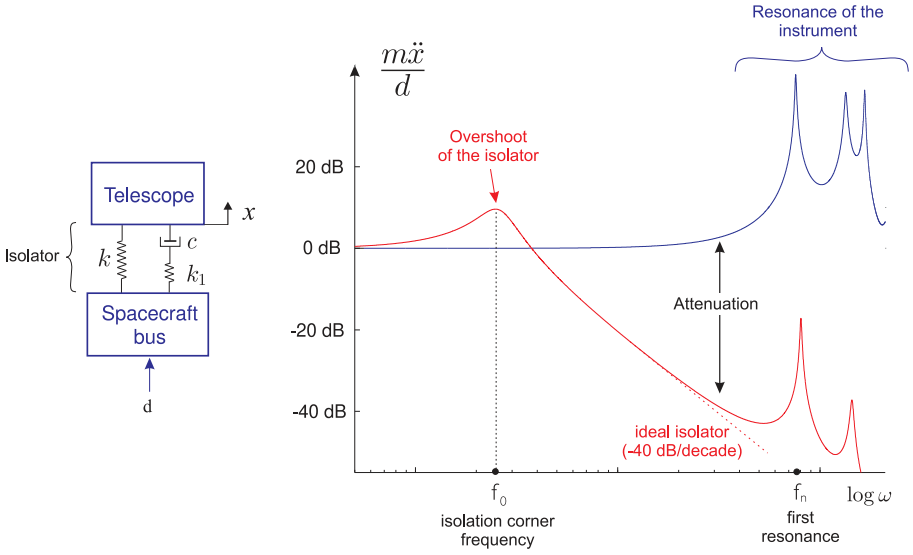

Figure 1: Effect of the isolator on the transmissibility between the spacecraft bus and the telescope.

1.2 Gough-Stewart platform

To fully isolate two rigid bodies with respect to each other, six single-axis isolators judiciously placed are needed. For a number of space applications, generic multi-purpose isolators have been developed with a standard Gough-Stewart platform architecture [4], in which every leg of the platform consists

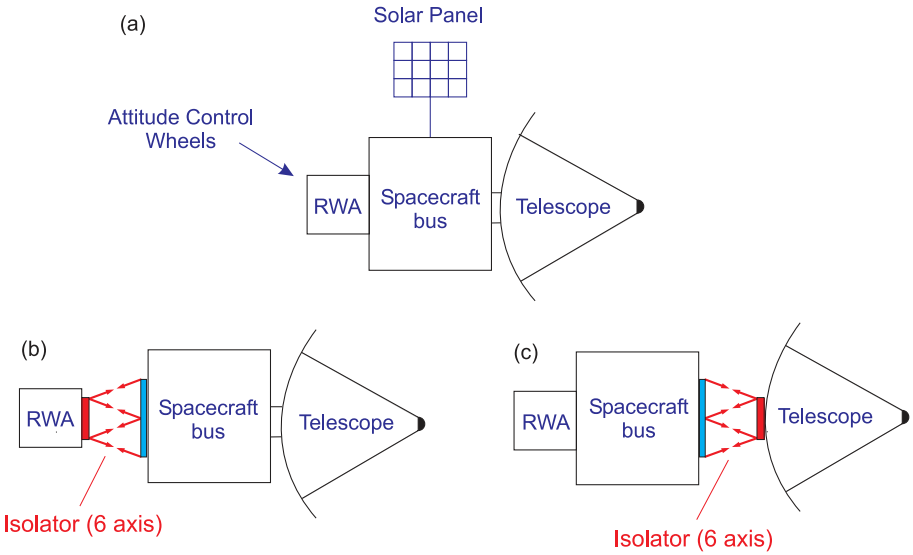

Figure 2: Spacecraft architecture. (a) Without isolator. (b) Isolator placed between the Reaction Wheel Assembly (RWA) and and the spacecraft bus. (c) Isolator between the spacecraft bus and the telescope.

of a single-axis active isolator, connected to the base plates by spherical joints. In the cubic architecture [5], the legs are mutually orthogonal, which minimizes the cross coupling between them. This configuration is particularly attractive, because it also has uniform stiffness properties and uniform control capability, and it has been adopted in most of the projects [6-16].

1.3 Passive vs. active isolation

The single-axis damped linear isolator has a high frequency attenuation rate of -20 dB/decade [17]; the overshoot at the corner frequency can only be reduced at the expense of reducing the high frequency isolation. This would mean a frequency gap of two decades to achieve an attenuation of 100. This problem can be solved by active control; the *sky-hook damper* [18,19] combines an undamped linear isolator with a feedback control based on the absolute velocity of the payload (obtained from a geophone or an accelerometer). This allows to control the overshoot of the isolator while maintaining a high frequency decay rate of -40 dB/decade. The stability of the sky-hook controller is guaranteed (infinite gain margin) when the isolator connects two rigid bodies, but not any more if one of them is flexible [20]. However, the sky-hook controller may also be implemented with a force feedback (Fig.3), and, in this case, the open-loop transfer function of the control system has *alternating poles and zeros* [21]. This important property is the key to robustness in active control of flexible structures. The control

architecture of Fig.3, with an Integral Force Feedback (IIF), $F_a = -(g/s)F$, generalizes the sky-hook damper to flexible structures; it has been applied in a decentralized manner in [16], with all loops having the same gain.

Robust active isolation [with respect to changes of structural parameters] is possible, and produces an attenuation rate of -40 dB/decade, but it is complicated, because it requires 6 actuators, 6 sensors and the control electronics. The following section discusses the *relaxation isolator* which is a passive isolator with an attenuation rate of -40 dB/decade.

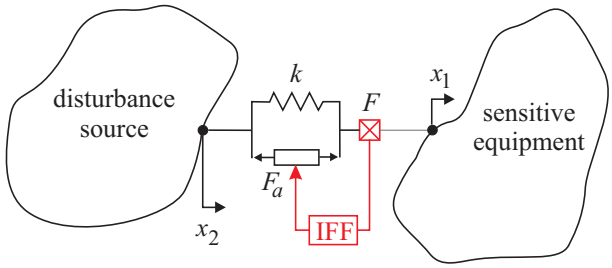

Figure 3: Two arbitrary flexible structures connected by a single-axis soft isolator with force feedback. The open-loop transfer function F/F_a exhibits alternating poles and zeros.

2 Relaxation isolator

The *relaxation* isolator (Fig.4.a) consists of a spring k in parallel with a Maxwell unit (damper c and spring k_1 in series) [22]. The governing equations are

$$M\ddot{x} + k(x - x_0) + c(\dot{x} - \dot{x}_1) = 0 \tag{2}$$

$$c(\dot{x} - \dot{x}_1) = k_1(x_1 - x_0) \tag{3}$$

or, in matrix form using the Laplace variable s,

$$\begin{bmatrix} Ms^2 + cs + k & -cs \\ -cs & k_1 + cs \end{bmatrix} \begin{Bmatrix} x \\ x_1 \end{Bmatrix} = \begin{Bmatrix} k \\ k_1 \end{Bmatrix} x_0 \tag{4}$$

It follows that the transmissibility reads

$$\frac{x}{x_0} = \frac{(k_1 + cs)k + k_1 cs}{(Ms^2 + cs + k)(k_1 + cs) - c^2 s^2} = \frac{(k_1 + cs)k + k_1 cs}{(Ms^2 + k)(k_1 + cs) + k_1 cs} \tag{5}$$

For large s, it behaves as $\sim s^{-2}$; this means that the asymptotic decay rate for large frequencies is -40 dB/decade. Physically, this corresponds to the fact that, at high frequencies, the viscous damper tends to be blocked, and the system behaves like a undamped isolator with two springs acting in parallel. Figure 5 compares the transmissibility curves for fixed values

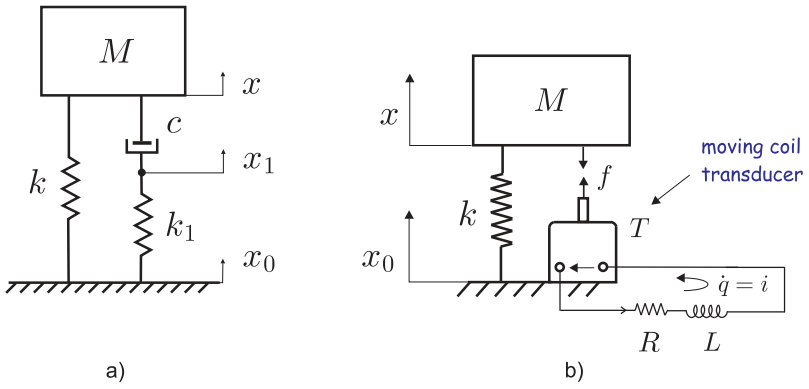

Figure 4: (a) Relaxation isolator consisting of a spring in parallel with a Maxwell unit. (b) Electromagnetic realization with a voice-coil and a $R-L$ circuit.

of k and k_1 and various values of c. For $c = 0$, the relaxation isolator behaves like an undamped isolator of natural frequency $\omega_n = (k/M)^{1/2}$. Likewise, for $c \to \infty$, it behaves like an undamped isolator of frequency $\Omega_n = [(k + k_1)/M]^{1/2}$. In between, the poles of the system are solution of the characteristic equation

$$(Ms^2 + k)(k_1 + cs) + k_1 cs = (Ms^2 + k)k_1 + cs(Ms^2 + k + k_1) = 0$$

which can be rewritten in root-locus form

$$1 + \frac{k_1}{c} \frac{s^2 + \omega_n^2}{s(s^2 + \Omega_n^2)} = 0 \tag{6}$$

For fixed values of ω_n and Ω_n, when the parameter k_1/c is changed[2], the poles of the system move along the root locus of Fig.6. The optimum value (producing the system poles with maximum damping ratio) is achieved for[3]

$$\frac{k_1}{c} = \frac{\Omega_n^{3/2}}{\omega_n^{1/2}} \tag{7}$$

and the corresponding damper constant is

$$c_{opt} = \frac{k_1}{\Omega_n}(\frac{\omega_n}{\Omega_n})^{1/2} = \frac{k_1}{\Omega_n}(1 + \frac{k_1}{k})^{-1/4} = \frac{k_1}{\omega_n}(1 + \frac{k_1}{k})^{-3/4} \tag{8}$$

The transmissibility corresponding to c_{opt} is also represented in Fig.5; it is nearly maximum at A.

[2] k_1/c is the inverse of the relaxation constant; it has the dimension of a frequency.
[3] see [21], p.106, where this root locus is analyzed in detail.

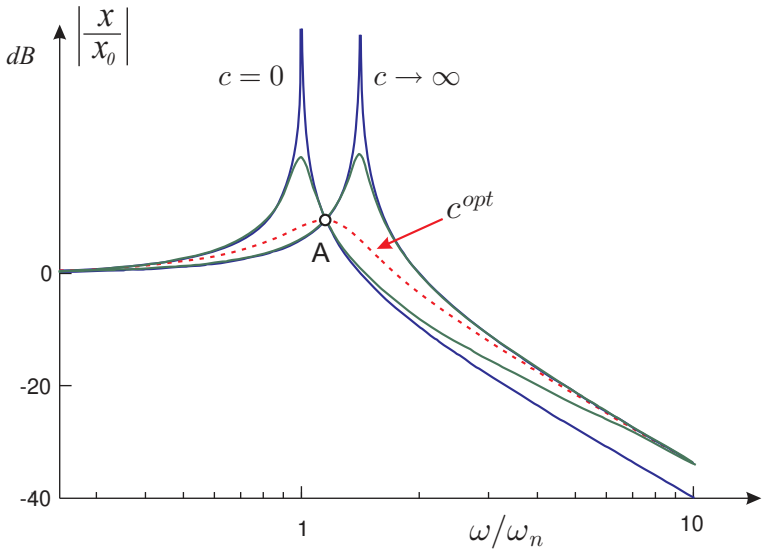

Figure 5: Transmissibility of the relaxation oscillator for fixed values of k and k_1 and various values of c. The first peak corresponds to $\omega = \omega_n$; the second one corresponds to $\omega = \Omega_n$. All the curves cross each other at A and have an asymptotic decay rate of -40 dB/decade. The curve corresponding to c_{opt} is nearly maximum at A.

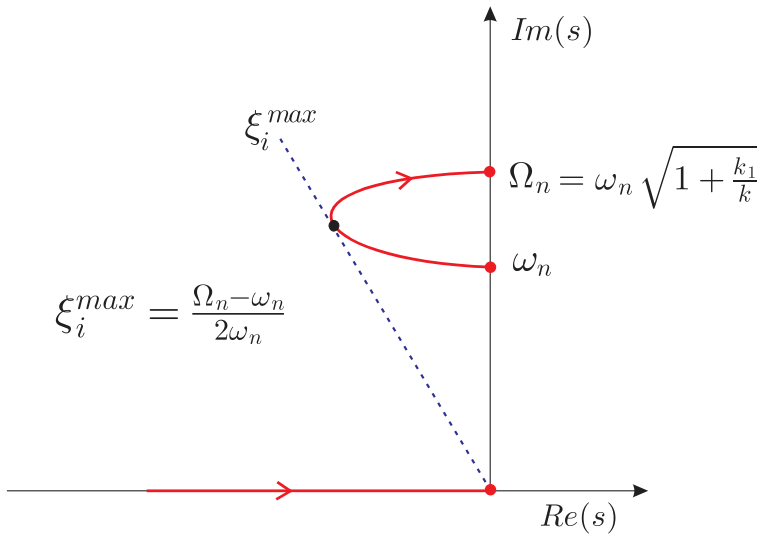

Figure 6: Root-locus of the solutions of Equ.(6) as c goes from zero to infinity. The maximum damping is achieved for $k_1/c = \Omega_n^{3/2}/\omega_n^{1/2}$.

The relaxation isolator can be realized with viscoelastic materials. However, the viscoelastic properties tend to vary widely with the large temperature variations typical of space environnement. A space qualified isolator using a fluid damper is presented in [23]; this "D-strut" was apparently used to isolate the reaction wheels of the Hubble space telescope. In [24], the D-strut has been combined in parallel with a voice coil actuator to produce an active strut for isolation and vibration suppression of precision payloads.

In this study, we propose a very simple way to realize a relaxation isolator with electrical components. The Maxwell unit is obtained with a moving coil transducer (voice coil) connected to a $R-L$ circuit.

2.1 Electromagnetic realization

Consider the electromechanical system of Fig.4.b, consisting of a spring k in parallel with a moving coil transducer[4] connected to an inductor L and a resistor R. If we adopt the electric charge q as electrical variable, the governing equations of the system are

$$M\ddot{x} + k(x - x_0) - T\dot{q} = 0 \tag{9}$$

$$L\ddot{q} + T(\dot{x} - \dot{x}_0) + R\dot{q} = 0 \tag{10}$$

or, in matrix form using the Laplace variable,

$$\begin{bmatrix} Ms^2 + k & -Ts \\ Ts & Ls^2 + Rs \end{bmatrix} \begin{Bmatrix} x \\ q \end{Bmatrix} = \begin{Bmatrix} k \\ Ts \end{Bmatrix} x_0 \tag{11}$$

It follows that the transmissibility reads

$$\frac{x}{x_0} = \frac{(Ls + R)k + T^2 s}{(Ms^2 + k)(Ls + R) + T^2 s} \tag{12}$$

Comparing with Equ.(5), one sees that the electromechanical isolator behaves exactly like a relaxation isolator provided that

$$\frac{Ls + R}{T^2} = \frac{cs + k_1}{k_1 c} \tag{13}$$

or

$$k_1 = \frac{T^2}{L} \qquad\qquad c = \frac{T^2}{R} \tag{14}$$

Thus, under these conditions, the two systems of Fig.4 have the same transmissibility.

Figure 7 compares the passive relaxation isolator with the active isolator. The force sensor has been removed and the control electronics eliminated.

[4] the constitutive equations of the moving coil transducer are $e = Tv$, $f = -Ti$, where e is the voltage drop in the coil (in the same direction as the current), v the relative velocity of the two parts, f is the external force required to balance the electromagnetic force, i is the current and T is the transducer constant, expressed in N/Amp or in Volt.sec/m.

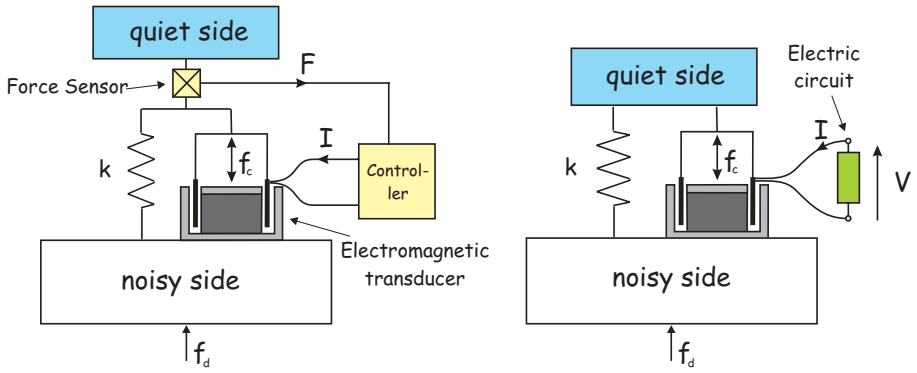

Figure 7: Comparison of the active isolator (left) with the passive isolator (right); if a RL electrical circuit is used, the passive isolator is a relaxation isolator; a purely resistive circuit produces a linear viscous isolator.

3 Six-axis isolator

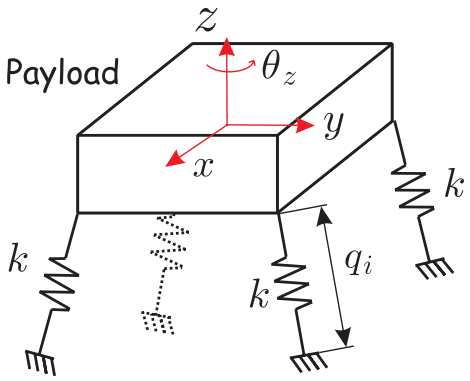

Figure 8: Six-axis isolator.

Let us consider a payload isolated by six identical isolators (Fig.8); if the isolators consist of simple springs of stiffness k, the six suspension modes are solution of an eigenvalue problem

$$(Ms^2 + K)\mathbf{x} = 0 \tag{15}$$

where $\mathbf{x}$ is a vector of 6 coordinates describing the position of the payload, e.g. $\mathbf{x} = (x, y, z, \theta_x, \theta_y, \theta_z)^T$. The mass matrix M can be obtained by writing the kinetic energy in terms of $\dot{\mathbf{x}}$. Similarly, the stiffness matrix is obtained by writing the strain energy in terms of $\mathbf{x}$. The strain energy in the system is $V = \frac{1}{2} k\, \mathbf{q}^T \mathbf{q}$, where $\mathbf{q} = (q_1, \ldots, q_6)^T$ is the vector of the spring extensions in the isolator and k is the stiffness common to all springs. If J is the Jacobian matrix connecting the spring extensions $\mathbf{q}$ to the coordinates $\mathbf{x}$ (J depends

on the topology of the isolator),

$$\mathbf{q} = J\mathbf{x} \tag{16}$$

one gets that

$$V = \frac{1}{2}k\ \mathbf{q}^T\mathbf{q} = \frac{1}{2}k\ \mathbf{x}^T J^T J\mathbf{x} \tag{17}$$

which means that the stiffness matrix is

$$K = kJ^T J \tag{18}$$

If the linear spring is replaced by a relaxation isolator, the common stiffness k must be replaced by the appropriate relationship between the spring force F and the spring extension $x - x_0$. From the constitutive equations of the isolator, (2) and (3), one finds easily that

$$\frac{F}{x - x_0} = k(s) = k[1 + \frac{k_1 cs}{k(k_1 + cs)}] \tag{19}$$

Thus, the (frequency-dependent) stiffness matrix of the six-axis relaxation isolator reads

$$K(s) = J^T J\ k[1 + \frac{k_1 cs}{k(k_1 + cs)}] = K[1 + \frac{k_1 cs}{k(k_1 + cs)}] \tag{20}$$

and the eigenvalue problem (15) becomes

$$\{Ms^2 + K[1 + \frac{k_1 cs}{k(k_1 + cs)}]\}\mathbf{x} = 0 \tag{21}$$

If ω_i and $\Phi = (\phi_1, \ldots, \phi_6)$ are the solution of the eigenvalue problem (15), normalized according to $\Phi^T M\Phi = I$, one can transform (21) into modal coordinates, $\mathbf{x} = \Phi\mathbf{z}$; using the orthogonality conditions, one finds a set of decoupled equations

$$s^2 + \omega_i^2[1 + \frac{k_1 cs}{k(k_1 + cs)}] = 0 \tag{22}$$

Upon introducing

$$\Omega_i^2 = \omega_i^2(1 + \frac{k_1}{k}) \tag{23}$$

the previous equation may be rewritten

$$\frac{k_1}{c}(s^2 + \omega_i^2) + s(s^2 + \Omega_i^2) = 0$$

or

$$1 + \frac{k_1}{c}\frac{s^2 + \omega_i^2}{s(s^2 + \Omega_i^2)} = 0 \tag{24}$$

which is identical to (6).

3.1 Modal spread

Thus, according to the foregoing equation, the six suspension modes follow independent root-loci connecting ω_i and Ω_i (Fig.9). However, k_1/c being a single scalar parameter, the optimal damping cannot be reached simultaneously in the six modes, because of the modal spread. A similar behavior was observed in the active isolator with decentralized control [6,16]. The best performance is achieved when the modal spread ω_6/ω_1 is low [6]. In the test structure described below, the six suspension modes are respectively 3.02 Hz, 3.02 Hz, 3.26 Hz, 6.66 Hz, 7.27 Hz, and 7.27 Hz, which limits the value of the modal spread to 2.4. The poles of the suspension modes are indicated by bullets in Fig.9.

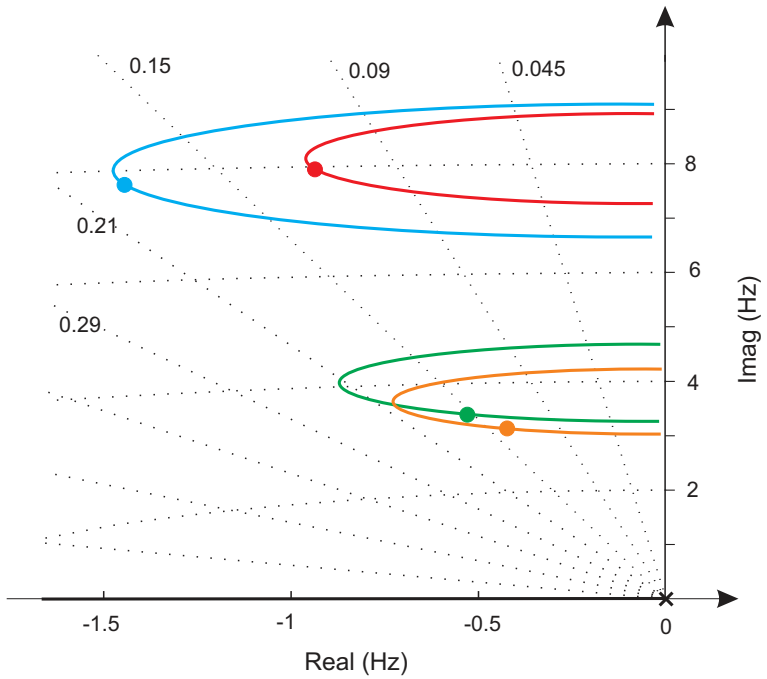

Figure 9: Root-locus of the six-axis relaxation isolator (there are only four different curves because of the symmetry of the system). The bullets correspond to the design values.

4 Hardware description

A six-axis passive isolator has been designed and built with a cubic Stewart platform architecture (Fig.10); the leg design is very similar to that of the active isolator described in [16], except that a force sensor is no longer necessary (which makes it lighter) and the voice coil transducer

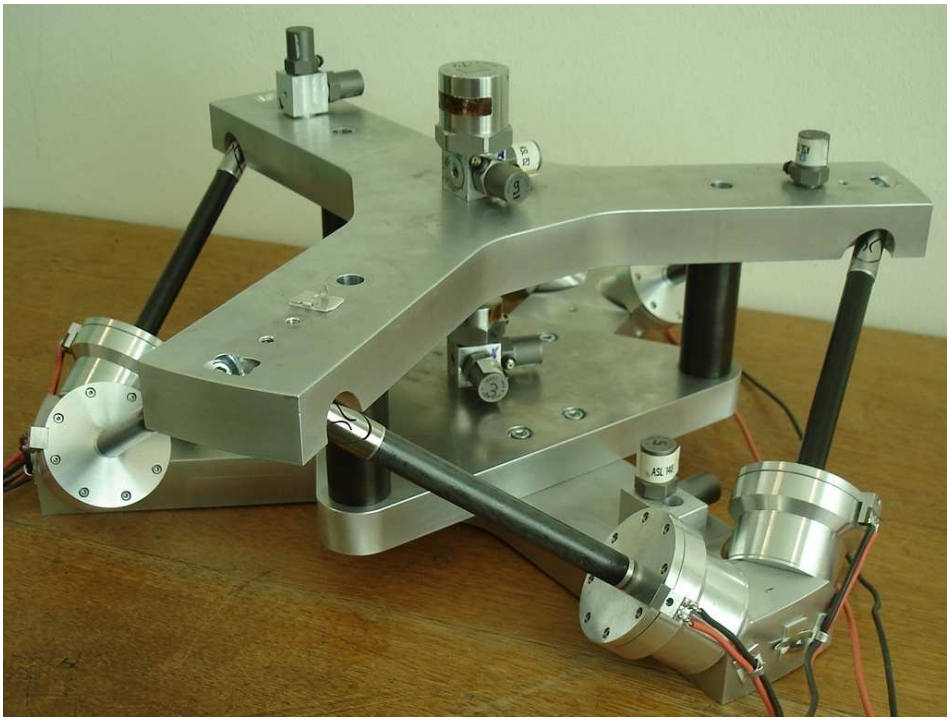

Figure 10: View of the isolator.

is significantly improved as explained below. The design of the new leg is shown in more detail in Fig.11.

4.1 Transducer

The transducer constant T and the electrical parameters R and L should be chosen according to (8) and (14), to achieve optimal performance. However, there is a difficulty associated with the intrinsic resistance of the voice-coil, R_c, and of the inductor, R_L. Indeed, if R_c+R_L is larger than the optimal circuit resistance, optimal damping of the structure cannot be achieved. We could not find any commercial transducer meeting the design requirements; a custom device was thus designed and built, based on magnetic FE simulations[5] to ensure that, for the required value of the transducer constant T, the coil resistance R_c is minimal. Keeping T as constant as possible over the stroke of the isolator is another challenge in the design. At the end of the process, R_c was reduced by a factor 6 with respect to the previous prototype (see [25] for details). The transduction constant T was measured to be 3.8 N/A, and the coil resistance $R_c = 1.65\,\Omega$, which are very close to the predicted values of 3.94 N/A and 1.51 Ω. Fig.12 shows the variation of

[5]with the freeware "FEMM", http://femm.foster-miller.net.

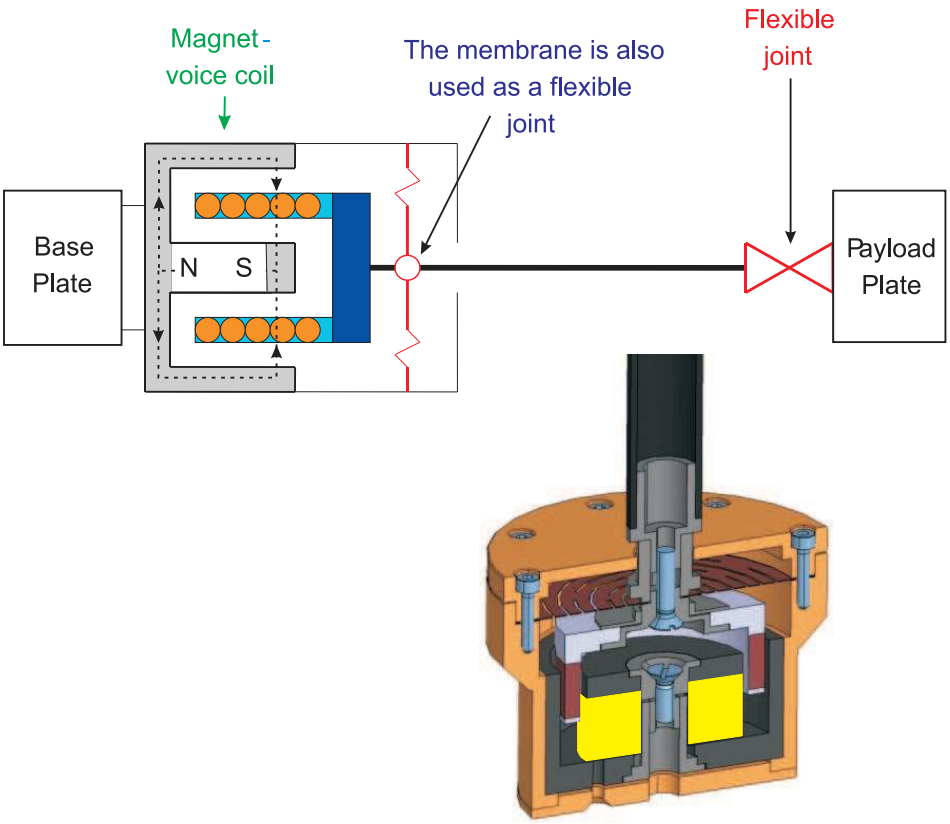

Figure 11: The leg of the passive isolator.

T with the axial displacement of the coil.

4.2 Inductor

The frequency ratio Ω_n/ω_n was selected to be approximately 1.5, which means that the ratio k_1/k is about 1.25. From (14), with the value of T given above, this corresponds to $L \simeq 29$ mH. Cheap inductors with such values are commercially available, e.g. by Epcos; the ones that we used have an inductance of about 27 mH and a very small series resistance R_L of about 0.25 Ω. Switches were placed such that the coils could be left open, shorted, or connected to the inductors. Note that, because of saturation and losses in the ferrite core, the inductors have a non-linear behavior with respect to the amplitude of the current that flows into them; this phenomenon is not fully understood but, for this application, the amplitude of the current was small and the non-linearity did not impact the results.

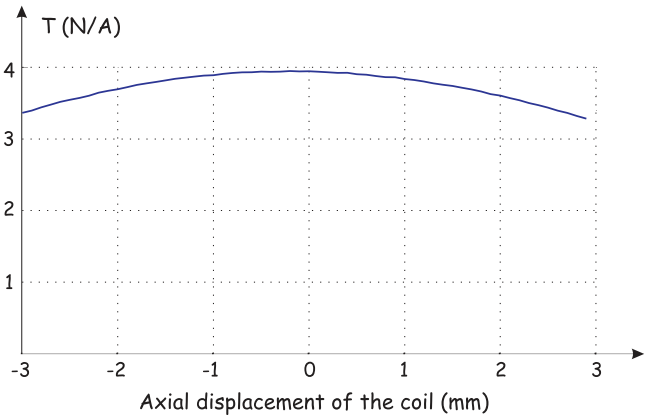

Figure 12: Evolution of the transducer constant T with the axial displacement of the coil (FE simulations).

5 Numerical simulations

A Finite Element model of the isolator was built in a way similar to [16]. In this study, however, the local modes of the membranes (300-500 Hz) are included in the model, in such a way that the model is accurate up to about 1 kHz. The model was used extensively to choose the characteristics of the transducers and of the inductors. Fig.13 to 16 show numerical predictions of the transmissibility. Two sets of curves are presented: the vertical transmissibility (Fig.13-14) and the the Fröbenius norm of the transmissibility matrix (Fig.15-16), which measures the global isolation capability of the isolator for every frequency [6,16].

Fig.13 compares the performances of the passive relaxation isolator (RL shunts) with that of the same isolator controlled with an Integral Force Feedback control law (decentralized sky-hook)[16]. The open-loop transmissibility (when the coil is open) is also shown for comparison. The IFF has less overshoot at the suspension modes, and it does not increase the corner frequencies of the system, but the weight of the force sensors in the legs decreases the frequency of the first local mode of the legs to about 400 Hz, and thus limits the high-frequency isolation. The relaxation isolator is effective between 5 Hz and 770 Hz and it achieves an impressive -50 dB isolation between 100 Hz and 500 Hz. Note the peaks at 300 Hz and 500 Hz, which are caused by internal resonances of the membranes: these peaks were not identified in [16], because in that study, the natural frequencies of the local modes of the legs were in the same frequency band.

Fig.14 and 16 compare the performance of the relaxation isolator with that when the coil is shorted ($L \simeq 0$). The R shunt has a lower decay rate than the RL shunt.

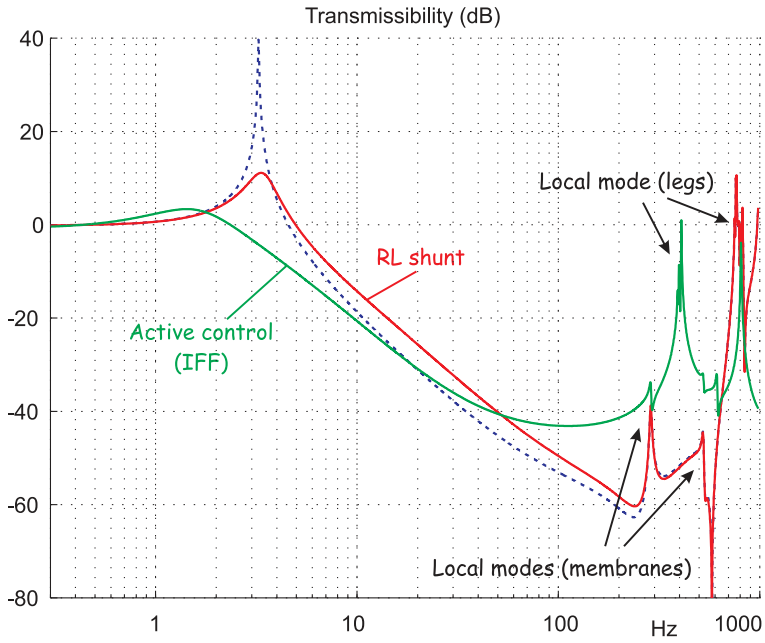

Figure 13: Numerical comparison of the vertical transmissibility: Open-loop (dotted line), relaxation isolator (RL shunt) and sky-hook (IFF).

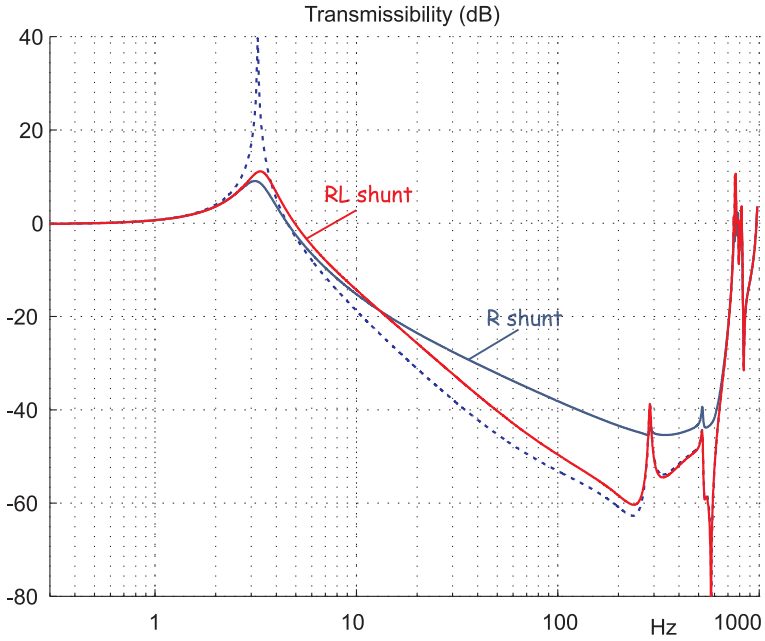

Figure 14: Numerical comparison of the vertical transmissibility: Open-loop (dotted line), relaxation isolator (RL shunt) and linear viscous (R shunt).

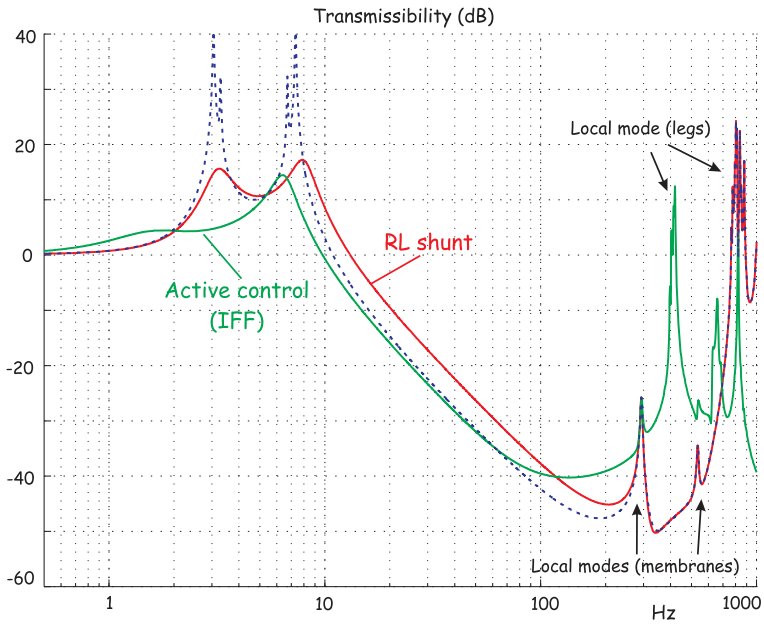

Figure 15: Numerical comparison of the transmissibility (Fröbenius norm of the transmissibility matrix): Open-loop (dotted line), relaxation isolator (RL shunt) and sky-hook (IFF).

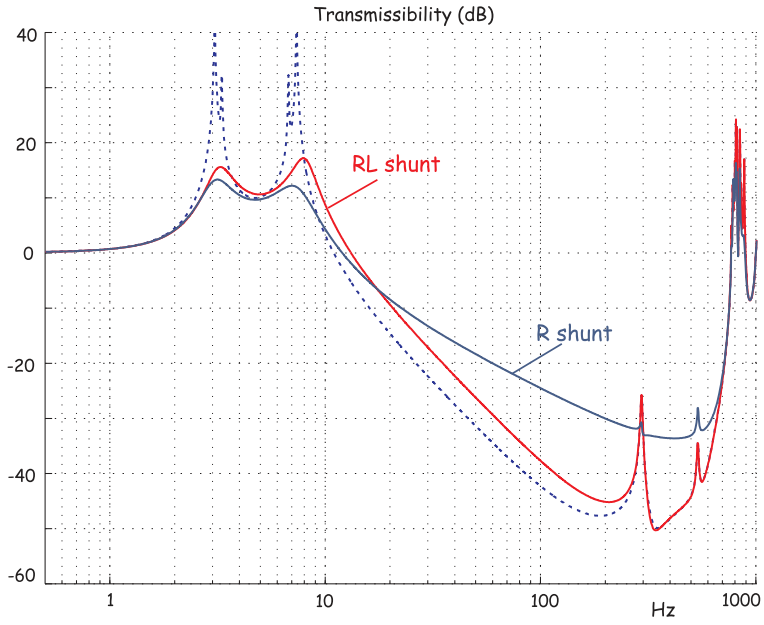

Figure 16: Numerical comparison of the transmissibility (Fröbenius norm of the transmissibility matrix): Open-loop (dotted line), relaxation isolator (RL shunt) and linear viscous (R shunt).

6 Experimental results

The isolator was tested in micro-gravity during the 48^{th} ESA parabolic flight campaign at Bordeaux-Mérignac (France). The identification procedure is exactly that described in [16]; there were about 90 parabolas providing 20 seconds of weightlessness each. Each measurement was repeated several times; next, the results were averaged in order to reduce the measurement noise. Fig.17.a shows the experimental vertical transmissibility when the coil is left open (open-loop), when it connected to the inductor (RL shunt) and when it is shorted (R shunt). Fig.17.b shows the coherence function which indicates the quality of the measurements. The numerical predictions of Fig.14 are also shown in dotted lines. The drop of coherence above 100 Hz is due to a low signal-to-noise ratio, mainly due to the isolator itself. Overall, the agreement is good.

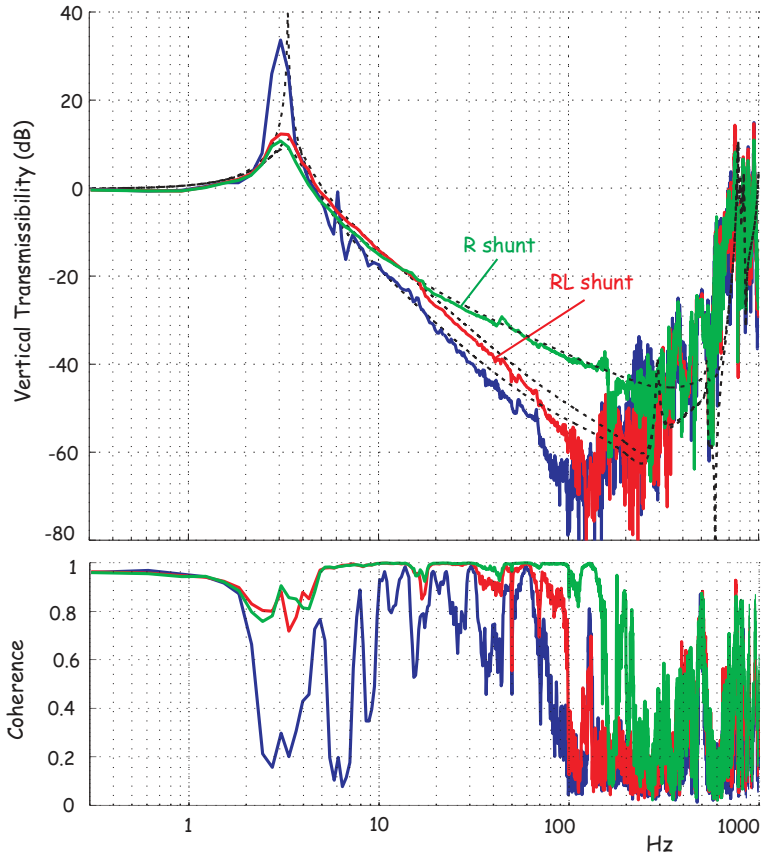

Figure 17: Experimental results. Vertical Transmissibility and coherence function(zero-g parabolic flight). The numerical predictions are in dotted lines.

7 Conclusions

A six-axis passive isolator has been designed and tested. The system is intended for the isolation of highly accurate payloads for space applications. The isolator consists of six identical legs mounted in a Stewart platform with cubic architecture; each leg is equipped with an electromagnetic transducer connected to a RL circuit. The system behaves like a relaxation isolator and its transmissibility exhibits an asymptotic decay rate of -40 dB/decade. The isolation performances have been found slightly better than that of an active isolator designed previously, based on a decentralized sky-hook controller. The isolator is efficient between 10 Hz and 750 Hz, with an attenuation exceeding 40 dB between 100 Hz and 500 Hz. However, the overshoot of the passive isolator is slightly larger than that of its active counterpart.

8 Acknowledgment

This study was supported by ESA/ESTEC in the framework of the program *PRODEX* (90147).

9 References

[1] Laskin, R.A., Sirlin, S.W., Future payload isolation and pointing system technology, *AIAA J. of Guidance and Control*, 9, 469-477, 1986.
[2] Collins, S.A., von Flotow, A.H., Active vibration isolation for spacecraft, 42^{nd} *IAF Congress*, paper No IAF-91-289, Montreal, Oct.1991.
[3] Bronowicki, A.J., Vibration Isolator for Large Space Telescopes, *AIAA J. of Spacecraft and Rockets*, vol.43, No 1, 45-53, January-February 2006.
[4] Stewart, D., A platform with six degrees of freedom, *Pro. Instn. Mech. Engrs.*, 180(15), 371-386, 1965-66.
[5] Geng, Z. Haynes, L., Six degree of freedom active vibration isolation system using the Stewart platforms, *IEEE Transactions on Control Systems Technology*, Vol.2, No 1, 45-53, 1994.
[6] Spanos, J., Rahman, Z., Blackwood, G., A soft 6-axis active vibration isolator, Proc. of the *IEEE* American Control Conference, 412-416, 1995.
[7] Rahman, Z.H, Spanos, J.T, Laskin, R.A., Multi-axis vibration isolation, suppression and steering system for space observational applications, *SPIE* Symposium on Astronomical Telescopes and Instrumentation, Kona-Hawaii, March 1998.
[8] Thayer, D., Vagners, J., von Flotow, A., Hardman, C., Scribner, K., Six-axis vibration isolationsystem using soft actuators and multiple sensors; *AAS 98-064*, 497-506, 1998.

[9] Thayer, D., Campbell, M., Vagners J., von Flotow, A., Six-Axis vibration isolation system using soft actuators and multiple sensors, *J. of Spacecraft and Rockets*, Vol.39, No 2, 206-212, March-April 2002.
[10] Hauge, G.S., Campbell, M.E., Sensors and control of a spaced-based six-axis vibration isolation system, *J. of Sound and Vibration*, 269, 913-931, 2004.
[11] McInroy, J.E., O'Brien, J.F., Neat, G.W., Precise, fault-tolerant pointing using a Stewart platform, *IEEE/ASME Transactions on Mechatronics,* Vol.4, No 1, 91-95, March 1999.
[12] McInroy, J.E., Neat, G.W., O'Brien, J.F., A robotic approach to fault-tolerant, precision pointing, *IEEE Robotics and Automation Magazine*, 24-37, Dec. 1999.
[13] McInroy, J.E., Hamann, J., Design and control of flexure jointed hexapods, *IEEE Transaction on Robotics,* 16(4), 372-381, August 2000.
[14] McInroy, J.E., Modeling and design of flexure jointed Stewart platforms for control purposes, *IEEE/ASME Transaction on Mechatronics,* 7(1), March 2002.
[15] Abu Hanieh, A., *Active Isolation and Damping of Vibrations via Stewart Platform*, PhD Thesis, ULB-Active Structures Laboratory, Brussels, Belgium, 2003.
[16] Preumont, A., Horodinca, M., Romanescu, I., de Marneffe, B., Avraam, M., Deraemaeker, A., Bossens, F., Abu Hanieh, A., A six-axis single stage active vibration isolator based on Stewart platform, *Journal of Sound and Vibration*, 300 : 644-661, 2007.
[17] Rivin, E.I., *Passive Vibration Isolation*, *ASME* Press, N-Y, 2003.
[18] Karnopp, D.C., Trikha, A.K., Comparative study of optimization techniques for shock and vibration isolation, *Trans. ASME, J. of Engineering for Industry, Series B*, 91, 1128-1132, 1969.
[19] Kaplow, C.E., Velman, J.R., Active local vibration isolation applied to a flexible telescope, *AIAA J. of Guidance and Control*, 3, 227-233, 1980.
[20] Preumont, A., François, A., Bossens, F., Abu-Hanieh, A., Force feedback versus acceleration feedback in active vibration isolation, *J. of Sound and Vibration*, 257(4), 605-613, 2002.
[21] Preumont, A., *Vibration Control of Active Structures, An Introduction*, 2nd Edition, Kluwer, 2002.
[22] Bourcier de Carbon, Ch., Perfectionnement à la suspension des véhicules routiers. Amortisseur à relaxation. Comptes Rendus de l'Académie des Sciences de Paris, Vol.225, pp. 722-724, Juillet-Déc. 1947.
[23] Hyde, T.T. and Anderson, E.H., Actuator with built-in viscous damping for isolation and structural control, *AIAA J.*, vol. 34(1), 129-135, 1996.
[24] Cobb, R.G., Sullivan, J.M., Das, A., Davis, L.P., Hyde, T.T., Davis, T., Rahman, Z.H., Spanos, J.T., Vibration isolation and suppression system for precision payloads in space, *Smart Mater. Struct.* vol.8, 798-812, 1999.

[25] de Marneffe, B. *Active and Passive vibration isolation and damping via shunted transducers*, PhD Thesis, ULB-Active Structures Laboratory, Brussels, Belgium, 2007.